JOURNAL OF VIROLOGY, June 2005, p. 7195–7206 Vol. 79, No. 11
0022-538X/05/$08.00+0 doi:10.1128/JVI.79.11.7195–7206.2005

Identification and Characterization of the Putative Fusion Peptide of the Severe Acute Respiratory Syndrome-Associated Coronavirus Spike Protein

Bruno Sainz, Jr.,[1] Joshua M. Rausch,[2] William R. Gallaher,[3] Robert F. Garry,[1] and William C. Wimley[2]*

Department of Microbiology and Immunology, Program in Molecular Pathogenesis and Immunity,[1] and Department of Biochemistry,[2] Tulane University Health Sciences Center, New Orleans, Louisiana 70112, and Department of Microbiology, Immunology and Parasitology, Louisiana State University Health Sciences Center, New Orleans, Louisiana 70112[3]

Received 28 October 2004/Accepted 5 January 2005

Severe acute respiratory syndrome-associated coronavirus (SARS-CoV) is a newly identified member of the family *Coronaviridae* and poses a serious public health threat. Recent studies indicated that the SARS-CoV viral spike glycoprotein is a class I viral fusion protein. A fusion peptide present at the N-terminal region of class I viral fusion proteins is believed to initiate viral and cell membrane interactions and subsequent fusion. Although the SARS-CoV fusion protein heptad repeats have been well characterized, the fusion peptide has yet to be identified. Based on the conserved features of known viral fusion peptides and using Wimley and White interfacial hydrophobicity plots, we have identified two putative fusion peptides ($SARS_{WW-I}$ and $SARS_{WW-II}$) at the N terminus of the SARS-CoV S2 subunit. Both peptides are hydrophobic and rich in alanine, glycine, and/or phenylalanine residues and contain a canonical fusion tripeptide along with a central proline residue. Only the $SARS_{WW-I}$ peptide strongly partitioned into the membranes of large unilamellar vesicles (LUV), adopting a β-sheet structure. Likewise, only $SARS_{WW-I}$ induced the fusion of LUV and caused membrane leakage of vesicle contents at peptide/lipid ratios of 1:50 and 1:100, respectively. The activity of this synthetic peptide appeared to be dependent on its amino acid (aa) sequence, as scrambling the peptide rendered it unable to partition into LUV, assume a defined secondary structure, or induce both fusion and leakage of LUV. Based on the activity of $SARS_{WW-I}$, we propose that the hydrophobic stretch of 19 aa corresponding to residues 770 to 788 is a fusion peptide of the SARS-CoV S2 subunit.

Severe acute respiratory syndrome (SARS) is a disease characterized by influenza-like symptoms, including fever, cough, dyspnea, and headache. The global outbreak of SARS began in the fall of 2002 in the Guangdong Province of China and gained worldwide attention due to its relative ease of transmission and disease severity. By July 2003, 8,098 probable cases had been reported, resulting in 774 deaths in 29 countries worldwide (33). The etiological agent of SARS was quickly identified as a newly emerged coronavirus (CoV) that is genetically distinct from previously characterized members of the *Coronaviridae* family (20, 45, 60).

Coronaviruses are large positive-strand RNA viruses with a broad host range (47, 74). Like other enveloped viruses, CoVs enter target cells by fusion between the viral and cellular membranes, a process mediated by the viral spike (S) protein (25). The CoV S protein, as characterized to date, consists of two noncovalently associated subunits, S1 and S2. The S1 subunit of the S glycoprotein mediates receptor binding (12, 82), while the S2 subunit is responsible for driving viral and target cell membrane fusion (83). The S2 subunit is a prototypical class I viral fusion protein containing common structural features (11, 26-28, 92) such as (i) a hydrophobic fusion peptide (50, 51), (ii) a pair of extended α-helices, specifically 4,3-hydrophobic heptad repeats (HR) (7, 97), and (iii) a cluster of aromatic amino acids proximal to (iv) a hydrophobic transmembrane anchoring domain.

Although the SARS-CoV S protein shares only 20 to 27% amino acid (aa) homology with the S proteins of other CoVs (69), recent studies have confirmed that the putative SARS-CoV S2 subunit is also a class I viral fusion protein. Using computational analysis, Gallaher and Garry (29) first proposed that the portion of the SARS-CoV S protein corresponding to the S2 subunit fit the prototypical model of a class I viral fusion protein based on the presence of two predicted HR regions at the N and C termini of S2 and an aromatic-aa-rich region just prior to the transmembrane anchor domain. Using synthetic peptides analogous to the two HR regions of S2, several groups have demonstrated that SARS-CoV HR1 and HR2 interact with one another to assume a coiled coil conformation (6, 49, 84, 99). Most recently, Xu et al. showed by crystal structure analysis that the SARS-CoV S protein fusion core forms a typical six-helix coiled coil bundle (98), as seen with the murine hepatitis virus (MHV) S protein (97). Furthermore, we have shown that the aromatic-aa-rich region of the SARS-CoV S2 subunit has similar functionality to the aromatic regions of both the human immunodeficiency virus (HIV) transmembrane (TM) glycoprotein (GP) (80) and Ebola virus (EboV) GP2 (71), in that peptides analogous to this aromatic region can induce the permeabilization of lipid vesicles (73). Al-

* Corresponding author. Mailing address: Department of Biochemistry, Tulane University Health Sciences Center, 1430 Tulane Avenue, SL-43, New Orleans, LA 70112. Phone: (504) 988-7076. Fax: (504) 988-2739. E-mail: wwimley@tulane.edu.

though the putative fusion peptide of the SARS-CoV S2 subunit has yet to be identified, it has been predicted that the SARS-CoV S fusion peptide lies within the N-terminal region of the S2 portion (residues 851 to 882), preceding HR1 (84).

Like other enveloped viruses encoding class I viral fusion proteins (27, 28), it is presumed that SARS-CoV uses membrane fusion mechanisms for viral entry (98, 99). After binding of the SARS-CoV S1 subunit to the mammalian receptor angiotensin-converting enzyme 2 (ACE2) (48, 85, 95) and/or CD209L (L-SIGN) (44), a conformational change in the S protein results in the exposure of an unidentified hydrophobic fusion peptide within S2. As with other class I viral fusion proteins (27, 28), the fusion peptide is believed to penetrate the target cell membrane, initiating the virion-cell membrane fusion event. Numerous mutagenesis studies of other enveloped viruses encoding class I viral fusion proteins (8, 23, 32, 38, 43, 51), as well as synthetic peptide studies (1, 14, 15, 17, 21, 34, 46, 58, 59, 62, 63, 66, 70), have provided substantial evidence of the role of the fusion peptide in initiating membrane fusion. Following insertion of the fusion peptide into the target cell membrane, HR interactions between residues 916 to 950 of HR1 and residues 1151 to 1185 of HR2 (84) mediate the formation of a six-helix coiled coil bundle (98, 99). The formation of this structure, also known as the trimer of hairpins, is believed to facilitate the apposition of both the viral and target cell membranes, resulting in fusion and subsequent entry of the viral core into the target cell.

Class I viral fusion proteins generally contain one fusion peptide, located (i) internally (27, 34, 38), as seen for avian sarcoma virus (ASV) TM and EboV GP2, or (ii) either at or near the N terminus of the protein, as seen for HIV TM and influenza virus hemagglutinin (HA) (28, 61, 66, 89). Variations in the number of aa and the position within the fusion protein are apparent between fusion peptides of different class I viral fusion proteins; however, distinct features are conserved. In general, fusion peptides are short (16 to 26 residues), hydrophobic sequences (8, 24, 88) that are rich in alanine, glycine, and phenylalanine residues (8, 26, 41). The presence of a canonical fusion tripeptide (YFG or FXG) is highly conserved among the fusion peptides of retroviruses, paramyxoviruses, influenza virus, and filoviruses (21, 26, 64, 70). It is believed that the canonical fusion tripeptide contributes to the functional organization of the fusion peptide itself (64). Lastly, the presence of a proline residue at or near the center of many fusion peptides has been implicated as critical for the interaction of the peptide with the target cell lipid membrane (19, 37, 43, 70). Taken together, the presence of these conserved features and the inherent hydrophobicity of fusion peptide sequences allow for their preferential interaction with lipid membranes.

For the present study, we identified the putative SARS-CoV fusion peptide by using synthetic peptides analogous to regions of the N terminus of the putative S2 subunit. We show here that a 19-aa synthetic peptide corresponding to residues 770 to 788 strongly partitions into the membranes of lipid vesicles and has a high propensity to adopt a β-sheet secondary structure. Furthermore, we demonstrate that this peptide alone induces membrane fusion of lipid vesicles and causes leakage of vesicle contents in a newly developed vesicle leakage assay. The data presented herein provide evidence of the presence of a putative fusion peptide at the N-terminal region of the SARS-CoV S2 protein and are consistent with previous findings using synthetic peptides to identify and characterize the fusion peptides of HIV gp41 and EboV GP2 (71, 78).

MATERIALS AND METHODS

Peptide synthesis. SARS-CoV fusion ($SARS_{WW-I}$ and $SARS_{WW-II}$) and SARS-CoV scrambled ($SARS_{WW-I-SCR}$) peptides were synthesized by a solid-phase methodology using a semiautomated peptide synthesizer and conventional *N*-alpha-9-fluorenylmethyloxycarbonyl chemistry by Genemed Synthesis, Inc. (San Francisco, Calif.). Peptides were purified by reversed-phase high-performance liquid chromatography, and their purity was confirmed by amino acid analysis and electrospray mass spectrometry. Peptide stock solutions were prepared in dimethyl sulfoxide (DMSO; spectroscopy grade), and their concentrations were determined spectroscopically (SmartSpec 3000; Bio-Rad, Hercules, Calif.).

LUV preparation. Large unilamellar vesicles (LUV) consisting of 1-palmitoyl-2-oleoyl-*sn*-glycero-3-phosphatidylcholine (POPC) with L-α-phosphatidylinositol (PI) from bovine livers (Avanti Polar Lipids, Birmingham, Ala.) and/or cholesterol (Sigma, St. Louis, Mo.) were prepared according to the extrusion method of Nayar and coworkers (54, 56). Briefly, lipids were dried from a chloroform solution with a nitrogen gas stream and a high vacuum overnight. Lipid vesicles used for peptide binding assays and fusion assays were resuspended in 5 mM HEPES, 100 mM NaCl, pH 7.4, to bring the concentration to 100 mM total lipid. For circular dichroism (CD) studies, lipid vesicles were resuspended in 10 mM potassium phosphate (PO_4), pH 7.0. Samples were subjected to repeated freezing and thawing for 15 cycles, followed by extrusion through 0.1-μm polycarbonate membranes in a Lipex Biomembranes extruder (Vancouver, British Columbia, Canada). For the preparation of terbium (III) chloride hexahydrate (Tb^{3+}) LUV, lipids were resuspended to a 100 mM concentration in 50 mM Tb^{3+}, 100 mM sodium citrate, and 10 mM *N*-Tris-(hydroxymethyl)methyl-2-amino ethane sulfonic acid (TES), pH 7.2. Gel filtration with Sephadex G-200 was used to remove unencapsulated Tb^{3+} in a buffer of 10 mM TES and 325 mM NaCl (67). Final lipid concentrations were determined by phosphate analysis (16, 22).

Peptide binding assay. The partitioning of peptides into the lipid bilayer was monitored by the fluorescence enhancement of tryptophan (91). Fluorescence was recorded at excitation and emission wavelengths of 280 and 340 nm, respectively, and with 8-nm bandwidths by use of an SML Aminco 8100 spectrofluorometer (Rochester, N.Y.). Quartz cuvettes with excitation and emission path lengths of 4 and 10 mm, respectively, were used. Measurements were carried out in 5 mM HEPES, 100 mM NaCl, pH 7.4. Peptides were added from stock solutions in DMSO to 250 μl of buffer and mixed by inversion. Likewise, LUV were titrated to a final lipid concentration of 1 mM and then mixed by inversion. Intensity values (I) were adjusted for lipid scattering and normalized to that of the peptide in buffer (I_o). Partitioning coefficients were obtained with equation 1, as follows:

$$I/I_o = 1 + \{(K_x \times [L])/([W] + K_x \times [L])\} \times [(I_{max}/I_o) - 1] \quad (1)$$

where K_x is a mole fraction partition coefficient that represents the amount of peptide in bilayers as a fraction of the total amount of peptide present in the system, I_{max} is a variable value for the fluorescence enhancement at complete partitioning determined by fitting the equation to the experimental data, $[L]$ is the concentration of lipid, and $[W]$ is the concentration of water (55.3 M).

Lipid vesicle fusion assay. Experiments to detect membrane fusion were performed by use of a fluorescence resonance energy transfer (FRET) technique for dye-labeled lipids (57, 77). In this assay, the fluorescence of one dye-labeled lipid, the donor, is quenched by the presence of another dye-labeled lipid, the acceptor, as long as they are confined to the same lipid membranes. Fusion with other unlabeled membranes dilutes the dye concentrations, and the quenching of the donor molecule is relaxed. FRET fusion assays employed 25 μM labeled 9:1 POPC:PI LUV with 7-nitro-2,1,3-benzoxadiazol-4-yl (NBD)-1-palmitoyl-2-oleoyl-*sn*-glycero-3-phosphatidylethanolamine (POPE) and rhodamine (Rho)-POPE (Avanti Polar Lipids) at a concentration of 1% mole fraction of total lipid each. Unlabeled 9:1 POPC:PI LUV were then added to the system to a total lipid concentration of 500 μM. Fluorescence spectra for these samples were recorded from 480 to 750 nm on an SLM Aminco 8100 spectrofluorometer, with excitation at 465 nm, in a 500-μl quartz cuvette. Time trace experiments of 1,000 s were conducted. The ability of peptides to increase NBD fluorescence was examined at peptide:lipid (P:L) ratios of 1:50, 1:25, and 1:10 beginning at 120 s. Prior to and following time trace spectra, the NBD fluorescence at 530 nm was measured to determine the pre- and postpeptide NBD fluorescence. Likewise, the use of 5%

Triton X-100 (Sigma) to permeabilize vesicles was used to normalize the NBD fluorescence of the system and to scale the resultant spectra for comparison.

Controls to determine the extent of fusion were prepared as separate LUV solutions representing serial twofold dilutions of dye concentrations within bilayers. LUV were prepared at NBD-Rho-POPE concentrations of 1.0%, 0.5%, 0.25%, 0.125%, and 0.0625% as well as with only 1.0% NBD-POPE or 1% Rho-POPE. These LUV were representative of 1, 3, 7, 15, and an infinite number of fusion events if all vesicles underwent uniform fusion with unlabeled LUV. Stocks of each of these labeled LUV solutions were prepared with unlabeled LUV to a final lipid concentration of 500 μM in proportions such that the overall number of each dye molecule was maintained. The NBD fluorescence of these solutions at 530 nm was determined and used to calculate the extent of membrane fusion observed upon the addition of peptide by the use of equation 2, as follows:

$$\% \text{ Fusion} = F/\{(0.52995 \times 0.18746) \times [1 - (F/0.52995)]\} \quad (2)$$

where F is equal to the NBD fluorescence normalized to the Triton X-100 control.

Lipid vesicle leakage assays. For microwell plate assays, a 200-μl aliquot of vesicle solution containing 500 μM Tb^{3+} LUV in 10 mM TES, 50 μM 2,6-pyridine dicarboxylic acid (DPA), and 325 mM NaCl, pH 7.2, was pipetted into each well of a plastic 8-by-12-format plate (67). Peptides in DMSO were added to each well at P:L molar ratios of 1:500, 1:250, 1:100, 1:50, and 1:25, the well contents were thoroughly mixed, and the plates were allowed to incubate at room temperature for 2 h. In addition to the peptide-treated wells, DMSO-treated and Triton X-100-treated wells served as negative and positive controls, respectively. After 2 h of incubation, Tb^{3+}/DPA fluorescence was visualized under horizontally mounted short-wave (254 nm) UV sources in a darkroom (67). Plates were photographed and images were recorded with a Nikon Coolpix 995 camera using a 4-s exposure time at 100 speed with a 2.6 aperture and a 540-nm band-pass optical filter between the sample and the lens. For each experimental plate, the Tb^{3+}/DPA fluorescence for the peptide-treated wells was compared to that of wells containing the same amount of untreated vesicles and of wells containing vesicles that had been lysed with the detergent Triton X-100. Color adjustment and contrasting were normalized to negative controls by the use of Adobe Photoshop.

To quantitate the extent of leakage observed in the Tb^{3+}/DPA microwell assay, we added peptides to 500 μM Tb^{3+} LUV in 10 mM TES, 50 μM DPA, and 325 mM NaCl, pH 7.2, at P:L molar ratios of 1:750, 1:500, 1:250, 1:100, 1:50, and 1:25. The samples were shaken at room temperature for 2 h, and the fluorescence of the samples was recorded at excitation and emission wavelengths of 270 nm and 490 nm, respectively, and with 8-nm bandwidths by use of an SML Aminco 8100 spectrofluorometer. Quartz cuvettes with excitation and emission path lengths of 4 and 10 mm, respectively, were used. The percent leakage of Tb^{3+} was calculated with equation 3 as follows:

$$\% \text{ Leakage} = [(F - F_o)/(F_{\max} - F_o)] \times 100 \quad (3)$$

where $F_{\max}$ is obtained by adding 25 μl 5% Triton X-100 and F_o is equivalent to the value for DMSO controls.

CD spectroscopy. CD spectra were recorded on a Jasco J-810 spectropolarimeter (Jasco Inc., Easton, Md.), using a 1-mm path length, 1-nm bandwidth, 16-s response time, and a scan speed of 10 nm/min. All CD runs were performed at room temperature with peptides dissolved in 10 mM PO_4 buffer at pH 7.0. LUV were added at a lipid concentration of 1 mM from a stock in 10 mM PO_4 buffer, pH 7.0. Three successive scans from 190 to 250 nm were collected, and the CD data are expressed as mean residue ellipticities, derived from the formula $\Theta = (\text{deg} \times \text{cm}^2)/\text{dmol}$.

Proteomic computational methods. Methods to derive general models of surface glycoproteins have been described previously (28). Domains with a significant propensity to form transmembrane helices were identified with TMpred (ExPASy; Swiss Institute of Bioinformatics) and Membrane Protein eXplorer (MPeX; Stephen White laboratory [http://blanco.biomol.uci.edu/mpex]). TMpred is based on a statistical analysis of TMbase, a database of naturally occurring transmembrane proteins (40), while MPeX detection of membrane spanning sequences is based on experimentally determined hydrophobicity scales (90, 94). Sequences with a propensity to partition into the lipid bilayer were also identified by MPeX, using interfacial settings.

RESULTS

Identification of putative fusion peptide(s) within the SARS-CoV S2 subunit. The Wimley and White interfacial hydrophobicity (WWIH) scale was used to initially identify regions of the SARS-CoV S2 subunit (N terminus) with a high propensity to partition into lipid membranes. This scale is based on the free energies of transfer (ΔG [kcal/mol]) of amino acid sequences from water to bilayer interfaces, taking into consideration the contribution from the peptide bond (94). Although no consensus exists regarding whether the SARS-CoV S protein is proteolytically cleaved into two noncovalently linked subunits (S1 and S2), the presence of a minimum furin cleavage site (R-X-X-R) (9, 55, 68) at residues 758 to 761 (R-N-T-R) suggests that the S glycoprotein may be proteolytically cleaved. The SARS-CoV S protein minimum furin cleavage site is not unlike the furin cleavage sites found in other CoV S proteins, such as the S proteins of MHV strain A59 (R-A-H-R) (52) and the human CoV OC43 (R-R-S-R), which can also be represented as R-X-X-R. Furthermore, recent studies to investigate SARS-CoV S protein processing reported that proteolytic processing of the viral glycoprotein is detectable in vitro (2, 96). As such, our analysis of the SARS-CoV S protein was limited to the putative S2 subunit (residues 762 to 1255).

Due to the salient similarities between the SARS-CoV S protein and the class I fusion proteins of other RNA viruses, we compared the interfacial hydrophobicity plot of the N-terminal region of the SARS-CoV S2 subunit to those of the N-terminal regions of HIV-1 gp41 and EboV GP2. For the N-terminal regions of the HIV-1 and EboV viral fusion proteins (Fig. 1A and B), a distinct region of high interfacial hydrophobicity was identified, corresponding to the experimentally determined fusion peptides of these two viral glycoproteins (1, 27, 34, 43, 59, 61, 64, 70, 79). For the SARS-CoV S2 subunit, however, two regions of high interfacial hydrophobicity were identified. Their positions within the S2 subunit N-terminal region are shown in Fig. 1C. The first region (WW-I), located 9 aa downstream of the minimum furin cleavage site (758R-N-T-R761), corresponds to residues 770MYKTPTLKY FGGFNFSQIL788 and has a predicted interfacial hydrophobicity score of 3.07 kcal/mol (Fig. 1C and Table 1). Its proximity to the presumed extreme N-terminal end of S2 is almost coincident with that of the fusion peptides of HIV-1, influenza virus, and paramyxoviruses. A second region (WW-II), located ~103 aa downstream of the minimum furin cleavage site, corresponds to residues 864ATAGWTFGAGAALQIPFAMQM AY886 and has a predicted interfacial hydrophobicity score of 3.76 kcal/mol (Fig. 1C and Table 1). This region more resembles the EboV GP2 (27) and ASV TM (38, 42) internal fusion peptides due to its distance from the furin cleavage site.

Sequence analyses of these two putative fusion peptides ($SARS_{WW\text{-}I}$ and $SARS_{WW\text{-}II}$) showed several conserved features that are shared with known viral fusion peptides. Both sequences are short, composed of mainly hydrophobic and nonpolar residues, and rich in alanine, glycine, and/or phenylalanine residues. Likewise, a putative canonical tripeptide or dipeptide with a central phenylalanine residue was present in both $SARS_{WW\text{-}I}$ and $SARS_{WW\text{-}II}$ (Table 1). Interestingly, $SARS_{WW\text{-}I}$ shares an identical canonical tripeptide with the EboV GP2 fusion peptide (Table 1). Another typical feature of

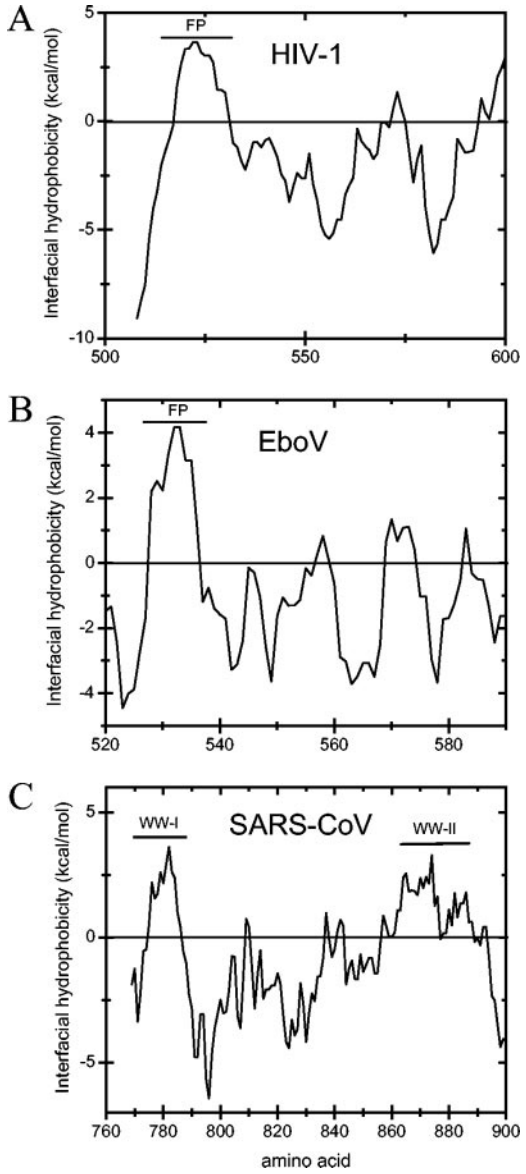

FIG. 1. Interfacial hydrophobicity plots corresponding to sequences of HIV-1 gp41, EboV GP2, and SARS-CoV S2. Interfacial hydrophobicity plots (mean values for a window of 19 residues) were generated by using the WWIH scales for individual residues (94) of HIV-1 strain HXB2 gp41 (amino acids 502 to 600) (A), EboV strain Zaire GP2 (amino acids 520 to 590) (B), and the SARS-CoV strain Urbani S2 subunit (amino acids 763 to 900) (C). The residues corresponding to the known fusion peptides of the HIV (A) and EboV (B) fusion proteins are indicated by black bars and labeled FP. In addition, the two putative SARS-CoV fusion peptides (C) studied in this work are indicated by black bar and are labeled $SARS_{WW-I}$ and $SARS_{WW-II}$.

fusion peptides is the presence of a proline residue at or near the center of the peptide (19, 37, 43, 70). Both $SARS_{WW-I}$ and $SARS_{WW-II}$ contain a proline residue 5 and 2 aa, respectively, from the center of the peptide (Table 1). Based on the WWIH plots (Fig. 1C) and the above conserved features, peptides analogous to these two regions of the S2 subunit were synthesized and examined for the ability to function independently as fusion peptides in the assays presented below.

SARS-CoV fusion peptide interacts with lipid membranes. A fundamental characteristic of viral fusion peptides is their inherent capacity to partition into lipid membranes. Therefore, we first assessed the ability of the two putative SARS-CoV fusion peptides to interact with membranes of LUV composed of POPC, PI, and/or cholesterol (CHOL). The degree to which a peptide partitions into a vesicle membrane can be determined fluorometrically by observing the change in tryptophan fluorescence (F) as a function of increasing lipid concentrations. The fluorescence of tryptophan increases in a low-polarity environment such as the lipid membrane interface. Figure 2 illustrates the tryptophan emission intensities of $SARS_{WW-I}$ and $SARS_{WW-II}$ in the presence of LUV composed of POPC and PI (9:1). Both peptides had similar fluorescence emission spectra in 10 mM HEPES buffer; however, only $SARS_{WW-I}$ showed a significant increase in tryptophan fluorescence accompanied by a negative shift in the maximum ($\Delta\lambda_{max} = 7$ nm) following the addition of 1,000 μM lipid (Fig. 2A). $SARS_{WW-II}$ fluorescence increased only slightly upon the addition of lipid, with a small negative shift in the maximum ($\Delta\lambda_{max} = 2$ nm) (Fig. 2B). Several studies have demonstrated a requirement for Ca^{2+} or Mg^{2+} in order for viral fusion peptides to partition into the membranes of lipid vesicles (59, 66, 70, 79). We observed no change in the tryptophan fluorescence of either peptide upon the addition of a divalent cation (5 mM Ca^{2+}) in the presence or absence of lipids. Emission spectra under these conditions were similar to those illustrated in Fig. 2 (data not shown).

The normalized tryptophan fluorescence (F/F_o) of the SARS-CoV putative fusion peptides was plotted as a function of increasing lipid concentrations to generate partition coefficients for each LUV tested (Table 2). Figure 3 illustrates a representative peptide-binding curve for $SARS_{WW-I}$, from which the partition coefficients were derived. The $SARS_{WW-I}$ peptide partitioned strongly into the membranes of all three LUV tested, with an increased preference for LUV containing the anionic lipid PI over LUV composed of only POPC. This result was not surprising, as numerous studies have shown that viral fusion peptides preferentially partition into membranes composed of anionic lipids such as PI or phosphatidylglycerol (59, 70). Consistent with the tryptophan emission spectra (Fig. 2B), the $SARS_{WW-II}$ peptide demonstrated minimal to nondetectable partitioning into LUV compared to the $SARS_{WW-I}$ peptide (Table 2). Although $SARS_{WW-II}$ scored favorably (3.76 kcal/mol) on the WWIH scale, fluorometric partitioning experiments do not easily detect peptide partitioning if the energy of partitioning is smaller than about 5 kcal/mol.

SARS-CoV fusion peptide induces fusion of lipid vesicles. By analogy to studies examining the ability of other synthetic viral fusion peptides to induce the fusion of lipid vesicles, the SARS-CoV putative fusion peptide would be expected to have a similar capacity. The induction of lipid membrane mixing by the peptides as a measure of fusogenic potential was measured by use of a FRET technique for dye-labeled lipids, which monitors the increase in NBD fluorescence following the fusion of labeled vesicles with unlabeled vesicles. Therefore, increases in NBD fluorescence are indicative of mixing of membrane lipids. Figure 4 illustrates the results of a time course experiment in which NBD fluorescence was measured pre- and postaddition of the SARS-CoV putative fusion pep-

TABLE 1. Amino acid sequences and WWIH scores of viral fusion peptides

Peptide[a]	Amino acid sequence[b]	Net charge	Position	WWIH score[c] (kcal/mol)
$SARS_{WW-I}$	M<u>W</u>KTPTLK**YFG**GFNFSQIL	+2	770–778	3.07
$SARS_{WW-II}$	ATAGWT**FG**AGAALQIPFAMQMAY	0	864–886	3.76
$SARS_{WW-I-SCR}$	MLFIK<u>W</u>GQYTNSPFLTKGF	+2	NA[d]	3.07
$EboV_{FP}$	GAAIGLAWIP**YFG**PAA	0	524–539	3.23
HIV_{FP}	AVGIGAL**FLG**FLGAAG	0	512–527	3.13

[a] The SARS fusion ($SARS_{WW}$) peptides were synthesized based on the amino acid sequence determined from GenBank accession no. AY278741 (SARS-CoV strain Urbani). The EboV fusion ($EboV_{FP}$) and HIV fusion (HIV_{FP}) peptide sequences were derived from references 70 and 59, respectively.
[b] Amino acid changes from tyrosine (Y) to tryptophan (W) are shown with underlining. The canonical fusion tripeptide is shown in bold.
[c] Interfacial hydrophobicity scores were determined according to the WWIH scale by use of a window of 19 residues.
[d] NA, not applicable.

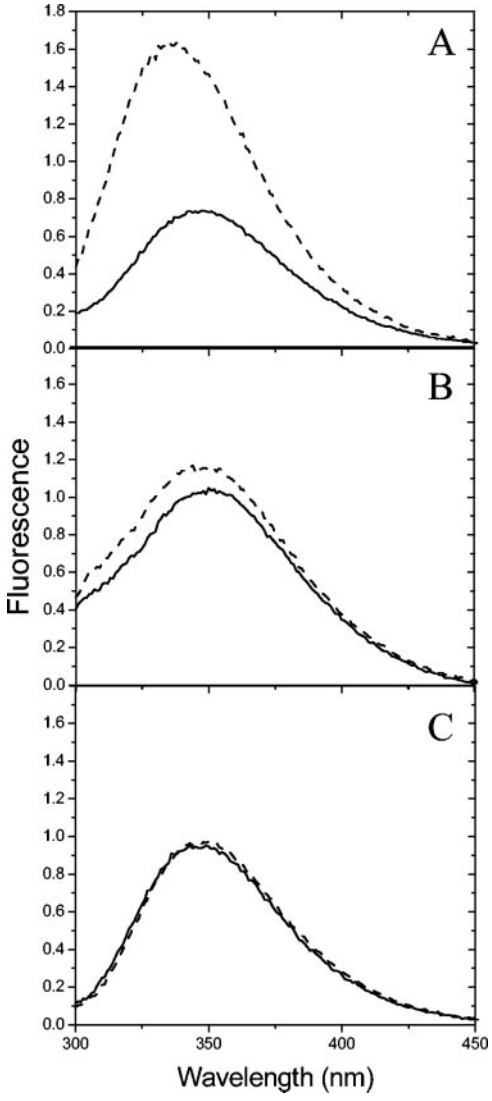

FIG. 2. Tryptophan fluorescence emission spectra of SARS-CoV fusion peptides. (A) $SARS_{WW-I}$; (B) $SARS_{WW-II}$; (C) $SARS_{WW-I-SCR}$. The peptides were incubated in 5 mM HEPES buffer alone (solid lines) or after the addition of LUV (dashed lines) composed of POPC and PI (9:1) (1,000 μM). The P:L molar ratio was 1:400.

tides to LUV composed of POPC and PI (9:1). Only after the addition of $SARS_{WW-I}$, but not $SARS_{WW-II}$, was there a rapid exponential increase in NBD fluorescence, followed by a plateau at 300 s post-peptide addition (Fig. 4, line b). Although $SARS_{WW-II}$ induced a marginal increase in NBD fluorescence over that of DMSO-treated vesicles (Fig. 4, line c versus line a), the extent and rate of fusion were not comparable to those with $SARS_{WW-I}$. Likewise, the addition of the divalent cation Ca^{2+} did not affect the capacity of either peptide tested to induce more or less NBD fluorescence (data not shown). Vesicle aggregation as a result of peptide-mediated fusion of lipid vesicles has been reported for several viral fusion peptides (59, 64, 66). Similar to these reports, we observed an aggregation of LUV after the addition of the $SARS_{WW-I}$ peptide at P:L molar ratios of 1:50 and higher; however, no vesicle aggregation was apparent after the addition of the $SARS_{WW-II}$ peptide at all P:L molar ratios tested (data not shown).

The experimental results in Table 3 summarize the extents of fusion observed for both $SARS_{WW-I}$ and $SARS_{WW-II}$ by use of the above-described FRET technique. The addition of $SARS_{WW-I}$ to LUV at P:L molar ratios of 1:50, 1:25, and 1:10 resulted in 38, 45, and 59% of the vesicles undergoing one fusion event. In contrast, the addition of $SARS_{WW-II}$ at equal P:L molar ratios resulted in only 11, 14, and 18% of the vesicles undergoing one fusion event. These data indicate that $SARS_{WW-I}$ has the capacity to induce effective mixing of lipid membranes, a function shared by other synthetic viral fusion peptides.

SARS-CoV fusion peptide induces leakage of lipid vesicles. To test the potential of the SARS-CoV fusion peptides to

TABLE 2. Partition coefficients of SARS-CoV peptides

LUV composition[a]	Partition coefficient[b] (10^3)		
	$SARS_{WW-I}$	$SARS_{WW-II}$	$SARS_{WW-I-SCR}$
POPC	38 ± 4	<10[c]	<10[c]
POPC-PI (9:1)	83 ± 17	<10[c]	<10[c]
POPC-PI-CHOL (6.5:1:2.5)	53 ± 27	<10[c]	<10[c]

[a] Lipids were titrated (100 μM to 1,000 μM) with 2.5 μM peptide in a volume of 500 μl.
[b] Partition coefficients were based on spectroscopic measurements of the change in tryptophan fluorescence as a function of increasing lipid titrations. Tryptophan intensity values (I) were fitted to equation 1, and the resulting partition coefficients are presented as means ± standard errors (n = 5 per group).
[c] Partitioning could not be definitively determined by means of the analysis described in Materials and Methods due to low tryptophan intensity values (I).

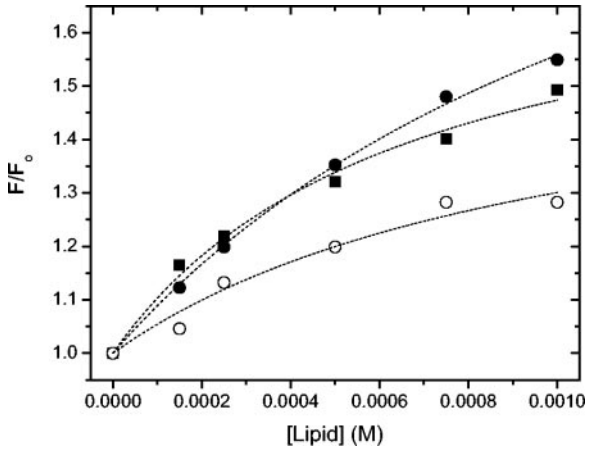

FIG. 3. $SARS_{WW-I}$ partitions into membranes of LUV. The graph shows changes in the tryptophan fluorescence of $SARS_{WW-I}$ as a function of increasing concentrations of LUV composed of POPC (■), POPC and PI (9:1) (●), or POPC, PI, and CHOL (6.5:1:2.5) (○). LUV were titrated at concentrations of 100, 250, 500, 750, and 1,000 μM lipid with 2.5 μM peptide. Tryptophan fluorescence values at each lipid titration (F) were normalized to tryptophan fluorescence values in 5 mM HEPES buffer alone (F_o).

perturb membrane integrity, we used a high-throughput leakage assay. The Tb^{3+}/DPA microwell assay is a sensitive visual screening assay developed to rapidly identify peptides capable of permeabilizing lipid membranes (67). The detection ability of the assay is based on the strong fluorescence emission of the lanthanide metal Tb^{3+} when it interacts with the aromatic chelator DPA. In the experimental assay, LUV containing encapsulated Tb^{3+} were added to a solution of 50 μM DPA in buffer. If the membrane integrity is compromised, Tb^{3+}/DPA fluorescence can be visually determined by the detection of bright green fluorescence upon irradiation with UV light. An

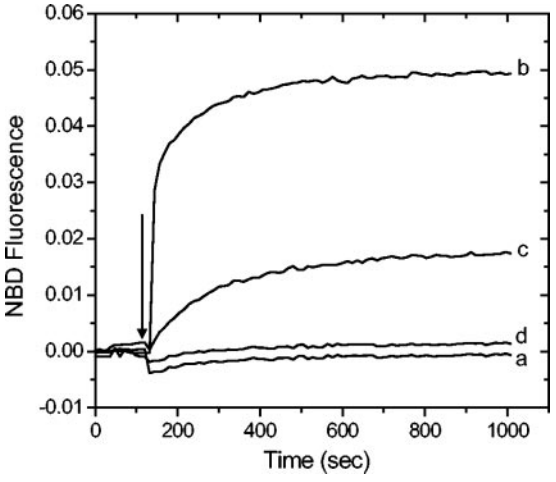

FIG. 4. $SARS_{WW-I}$ induces fusion of LUV. NBD fluorescence was detected by the FRET assay as a function of time. A DMSO control (a), $SARS_{WW-I}$ (b), $SARS_{WW-II}$ (c), or $SARS_{WW-I-SCR}$ (d) (P:L ratio of 1:10) was added to a 500 μM suspension of lipid composed of 25 μM POPC–PI–NBD-POPE–Rho-POPE LUV (8.8:1:0.1:0.1) and 475 μM POPC-PI LUV (9:1). The arrow indicates the time of addition of the peptides.

TABLE 3. $SARS_{WW}$-mediated fusion of LUV

Peptide	P:L ratio[a]	% Fusion with LUV[b]
$SARS_{WW-I}$	1:50	38
	1:25	45
	1:10	59
$SARS_{WW-II}$	1:50	11
	1:25	14
	1:10	18

[a] SARS-CoV peptides were added at various P:L molar ratios to 2.5 ml of LUV suspension containing 500 μM POPC–PI–POPE-NBD–POPE-Rho (8.8:1:0.1:0.1) vesicles.

[b] The data were fitted to equation 2 and are presented as percentages of vesicles that underwent one fusion event.

example plate is shown in Fig. 5A in which both $SARS_{WW-I}$ and $SARS_{WW-II}$ were tested for the potential to permeabilize LUV composed of POPC and PI (9:1) at various P:L molar ratios. The $SARS_{WW-I}$ peptide permeabilized vesicles at P:L ratios as low as 1:250, with extensive leakage detected at P:L ratios of 1:50 and 1:25 (Fig. 5A, row 1). The extent of leakage induced by $SARS_{WW-I}$ at a P:L ratio of 1:25 was comparable to the observed leakage of Triton X-100-solubilized wells (Fig. 5A, row 1 versus row 4). In contrast, leakage induced by the $SARS_{WW-II}$ peptide was minimal compared to that induced by the $SARS_{WW-I}$- and Triton X-100-treated groups and was only detectable at P:L ratios of 1:25 and 1:50 (Fig. 5A, row 2).

To further characterize the extent of leakage observed in the Tb^{3+}/DPA microwell assay, we measured Tb^{3+} fluorescence fluorometrically as described in Materials and Methods. A time trace experiment was initially performed to observe the rate of $SARS_{WW-I}$-induced leakage of Tb^{3+} encapsulated within LUV at P:L ratios of 1:100, 1:50, and 1:25 (Fig. 5B). Compared to the rate of NBD fluorescence observed in the fusion assay, $SARS_{WW-I}$ induced a slower exponential increase in Tb^{3+} fluorescence (Fig. 5B). Likewise, the lack of a plateau in Tb^{3+} fluorescence at 30 min post-peptide addition suggested that leakage was not complete. Therefore, for determination of the full extent of peptide-induced leakage of Tb^{3+} from LUV, the SARS-CoV fusion peptides were incubated at various P:L molar ratios, and after 2 h of incubation at room temperature, the extent of Tb^{3+} leakage from lipid vesicles was measured fluorometrically. As with the Tb^{3+}/DPA microwell assay, the $SARS_{WW-I}$ peptide induced Tb^{3+} leakage from LUV to a greater degree than did $SARS_{WW-II}$ at all P:L molar ratios tested. For example, $SARS_{WW-I}$ induced 20%, 46%, and 65% leakage of vesicle contents at P:L ratios of 1:100, 1:50, and 1:25, respectively. In contrast, the $SARS_{WW-II}$ peptide induced only 4%, 10%, and 15% leakage at the same P:L molar ratios. Taken together, the data presented above indicate that the $SARS_{WW-I}$ peptide efficiently disrupts membrane integrity, as evident by its ability to induce leakage in the Tb^{3+}/DPA assay.

A scrambled SARS-CoV fusion peptide is inactive. The data presented thus far demonstrate that of the two putative fusion peptides tested, only $SARS_{WW-I}$ is active in all three assays. This peptide not only fulfills the compositional requirements of a viral fusion peptide, but it demonstrates functional characteristics that have been identified for isolated fusion peptides of other class I viral fusion proteins (21, 26, 30). Therefore, in order to determine if the capacity of $SARS_{WW-I}$ to partition

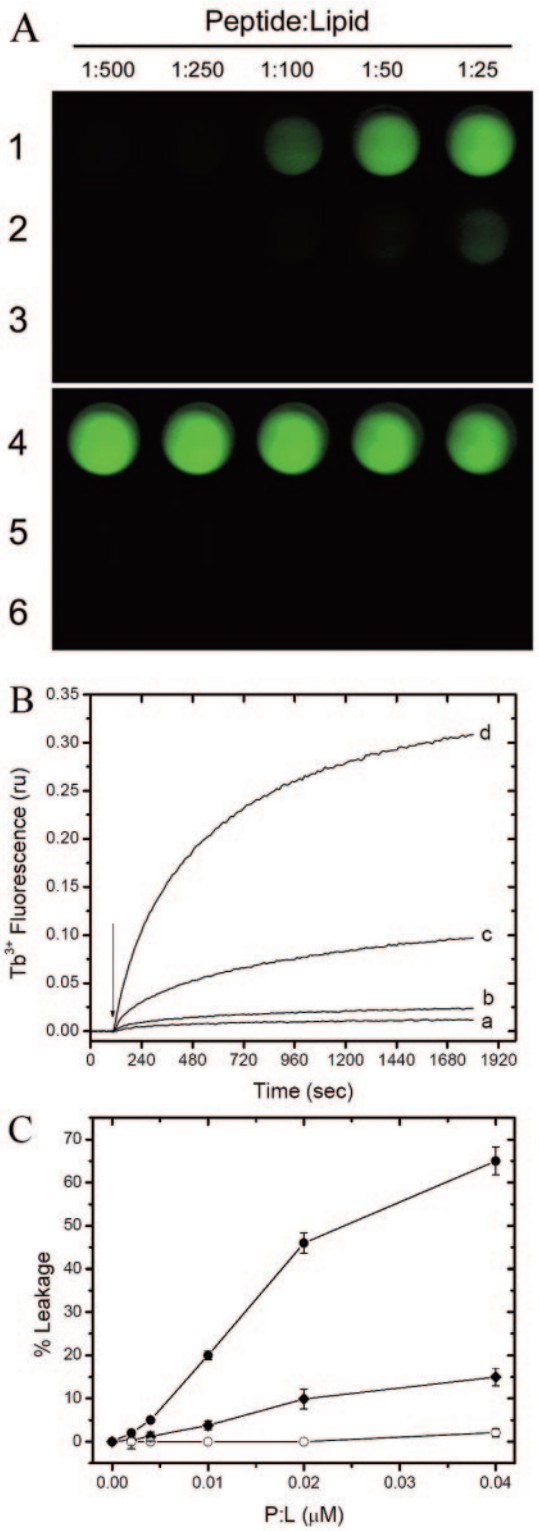

FIG. 5. $SARS_{WW-I}$ induces leakage of LUV contents. (A) Tb^{3+}/DPA microwell assay. Each well contained 250 μl of 50 μM DPA and 500 μM Tb^{3+}-encapsulated LUV composed of POPC and PI (9:1). The wells were treated with $SARS_{WW-I}$ (1), $SARS_{WW-II}$ (2), $SARS_{WW-I-SCR}$ (3) (P:L molar ratio of 1:500, 1:250, 1:100, 1:50, or 1:25), 20 μl of Triton X-100 (4), or 20 μl of DMSO (5) or were left untreated (6). The plates were incubated for 2 h at room temperature, and membrane permeabilization was determined by visual detection of Tb^{3+}/DPA fluorescence. (B) Time trace analysis of Tb^{3+} fluorescence after the addition of a DMSO control (a) or $SARS_{WW-I}$ at a P:L molar ratio of 1:100 (b), 1:50 (c), or 1:25 (d). The arrow indicates the time of addition of the peptides. (C) Extent of leakage from Tb^{3+}-encapsulated LUV. $SARS_{WW-I}$ (●), $SARS_{WW-II}$ (♦), or $SARS_{WW-I-SCR}$ (○) was added to LUV composed of POPC and PI (9:1) at the indicated P:L molar ratios. The samples were incubated at room temperature for 2 h before Tb^{3+} fluorescence was measured. The percent leakage was determined by using equation 3.

into lipid membranes and to induce both fusion and permeabilization of lipid vesicles is a property of the specific peptide sequence, we synthesized and tested a scrambled peptide in the aforementioned assays. The resulting scrambled peptide, $SARS_{WW-I-SCR}$, was identical in polarity, hydrophobicity, and aa composition to $SARS_{WW-I}$; however, the specific order of aa was arbitrarily rearranged and the canonical tripeptide was intentionally altered (Table 1). The ability of the $SARS_{WW-I-SCR}$ peptide to interact with membranes of LUV composed of POPC, PI, and/or CHOL was first assessed. Upon the addition of 1,000 μM lipid, no enhancement or shift in the maximum was detected, indicating minimal to no partitioning of the peptide into the membranes of the vesicles tested (Fig. 2C and Table 2). In addition, when tested for the ability to induce vesicle fusion, the $SARS_{WW-I-SCR}$ peptide, at a P:L molar ratio of 1:10, showed no significant increase in NBD fluorescence compared to DMSO-treated control samples (Fig. 4, line d versus line a). Again, when tested in the Tb^{3+}/DPA assay, the $SARS_{WW-I-SCR}$ peptide did not induce Tb^{3+} leakage (Fig. 5A, row 3, and C). The inability of the $SARS_{WW-I-SCR}$ peptide to partition into lipid membranes and to induce both fusion and permeabilization of lipid vesicles suggests that the aa sequence order is vital for the activity of the $SARS_{WW-I}$ peptide.

CD analysis of the SARS-CoV fusion peptide. To examine the potential for the formation of secondary structures upon interactions with lipid membranes, we examined the $SARS_{WW-I}$ peptide by CD spectroscopy. Figure 6 shows representative far-UV CD spectra of both the $SARS_{WW-I}$ and $SARS_{WW-I-SCR}$ peptides in buffer and with LUV. An analysis of $SARS_{WW-I}$ in 10 mM PO_4 buffer, pH 7.0, showed a β-sheet spectrum with a prominent minimum at 218 nm and a tryptophan minimum at 228 nm (93). Likewise, in the presence of 1 mM LUV composed of POPC and PI (9:1), the $SARS_{WW-I}$ peptide again showed a β-sheet spectrum, although the minimum at 218 nm was shifted to a slightly higher wavelength (Fig. 6A). The lack of a more defined minimum at 218 nm was most likely a result of the scattering effect attributed to the visible vesicle fusion and aggregation at the P:L molar ratios tested. To ensure that the $SARS_{WW-I}$ peptide assumed a well-defined β-sheet structure upon interaction with lipid vesicles at low peptide concentrations, at which vesicle aggregation was not apparent, we analyzed the 5 μM peptide in buffer and with LUV. A 32-s response time and a scan speed of 5 nm/min were used to obtain a reliable UV CD spectrum. Under these conditions, the $SARS_{WW-I}$ peptide showed a well-defined minimum at 218 nm in the presence of lipid, which is indicative of a transition to a β-sheet structure in membranes (Fig. 6A, inset). The $SARS_{WW-I-SCR}$ peptide was also examined by CD spectroscopy for the formation of secondary structures in

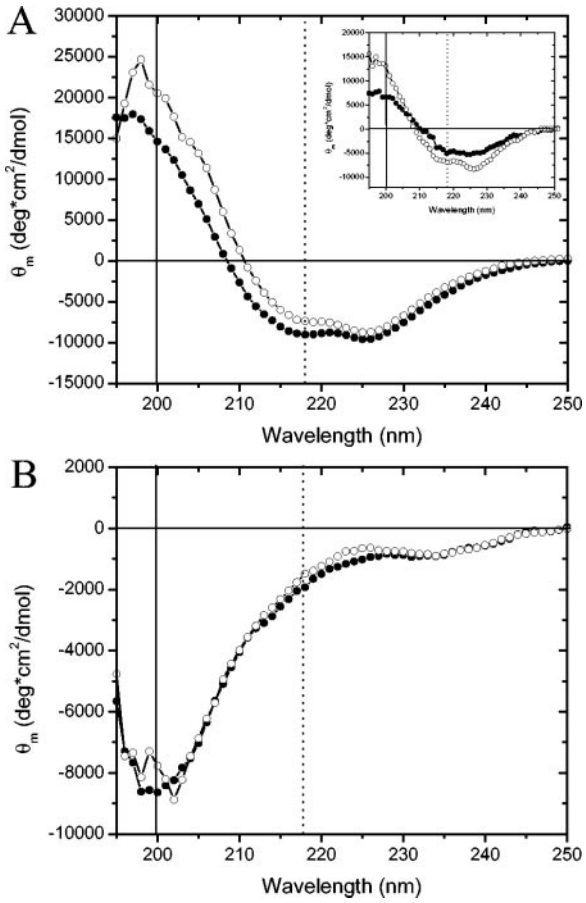

FIG. 6. $SARS_{WW-1}$ adopts a β-sheet conformation. The graphs show CD spectra (mean residue ellipticities [Θ]) of the SARS-CoV fusion peptides (50 μM) $SARS_{WW-I}$ (A) and $SARS_{WW-I-SCR}$ (B) in 10 mM PO_4 buffer, pH 7.0, alone (●) or with 1 mM LUV composed of POPC and PI (9:1) (○) at room temperature. Inset, CD spectra of $SARS_{WW-I}$ (5 μM) in 10 mM PO_4 buffer, pH 7.0, alone (●) or with 1 mM LUV composed of POPC and PI (9:1) (○) at room temperature. Settings were adjusted to a 32-s response time and a scan speed of 5 nm/min.

buffer and with LUV (Fig. 6B). This peptide did not partition into lipid membranes or induce membrane fusion or leakage; therefore, we examined whether scrambling the peptide sequence interfered with the formation of the secondary structure required for its function. No defined α-helical or β-sheet structure was apparent, as evident by the random coil spectra observed in buffer and upon the addition of LUV (Fig. 6B). These data suggest that the SARS-CoV fusion peptide has a sequence-specific propensity to adopt a β-sheet structure upon interaction with lipid membranes. In addition, it appears that the inability of the $SARS_{WW-I-SCR}$ peptide to functionally mimic $SARS_{WW-I}$ could be due, in part, to the loss of a defined secondary structure.

DISCUSSION

Dissecting the mechanisms by which the SARS-CoV S protein mediates fusion between the virion envelope and the cellular membrane could significantly contribute to our understanding of SARS-CoV pathobiology and to the design of antiviral drugs and vaccines. Recent studies have determined that the SARS-CoV S fusion protein is a prototypical class I viral fusion protein in that it contains two 4,3-hydrophobic HR regions responsible for the formation of a six-helix bundle, similar to the fusion proteins of EboV (53, 86, 87) and the lentiviruses HIV and simian immunodeficiency virus (10, 13, 53). The formation of this hairpin structure is believed to drive membrane fusion by mediating the juxtaposition of both the viral and cellular membranes. The formation of the six-helix bundle, however, is preceded by the insertion of a hydrophobic fusion peptide located within the N-terminal region of the fusion protein (36). Insertion of the fusion peptide into the target cell membrane facilitates both target cell membrane disruption and the subsequent formation of the six-helix bundle. Although studies by Luo and Weiss have identified putative fusion peptides of MHV (50, 51), no fusion peptide has been identified in the N-terminal region of the SARS-CoV S2 subunit.

Using the characteristics of known viral fusion peptides, including their hydrophobicity and aa composition and the presence of a canonical fusion tripeptide, we identified two putative fusion peptides with high interfacial hydrophobicities in the N-terminal region of the SARS-CoV S2 subunit (Fig. 1 and Table 1). $SARS_{WW-I}$ is located at the extreme N-terminal end of S2, 9 aa downstream of a minimum furin cleavage site. In viral fusion proteins that undergo proteolytic cleavage (e.g., HIV TM and influenza virus HA), fusion peptides are situated at the N-terminal region. Although it has not been conclusively determined whether the SARS-CoV S protein is proteolytically cleaved during maturation, a minimum furin cleavage site is present within the S protein (758R-N-T-R761), and recent studies reported that the SARS-CoV S protein is proteolytically cleaved in vitro (2, 96). Studies examining the conserved furin cleavage sites in other coronaviruses have shown conflicting results regarding whether cleavage is necessary for infectivity and/or cell-cell fusion (reviewed in reference 18). Most recently, de Haan et al. demonstrated that the S protein of MHV strain A59 is proteolytically cleaved; however, the requirements for cleavage during virion-cell and cell-cell fusion differ (18).

The second possible SARS-CoV fusion peptide, $SARS_{WW-II}$, is similar to the fusion peptides of EboV GP2 (27, 70) and ASV TM (27) and the internal fusion peptides of class II viral fusion proteins (31), as it is located distal to the furin cleavage site but still within the N-terminal region of S2. Despite their different locations within the S2 subunit, both $SARS_{WW-I}$ and $SARS_{WW-II}$ contain several features which are conserved among all known viral fusion peptides. For example, both demonstrated a high interfacial hydrophobicity when analyzed with the WWIH scale (Fig. 1C and Table 1), suggesting an inherent propensity to partition into lipid membranes (94). Similar regions of high interfacial hydrophobicity are apparent in the fusion proteins of HIV and EboV (Fig. 1A and B). Moreover, both $SARS_{WW-I}$ and $SARS_{WW-II}$ are rich in alanine, glycine, and/or phenylalanine residues and contain a canonical fusion tripeptide and a proline residue (Table 1), making both peptides potential fusion peptide candidates. Classifying $SARS_{WW-I}$ and $SARS_{WW-II}$ as internal or N-terminal putative fusion peptides will depend on deciphering whether and where

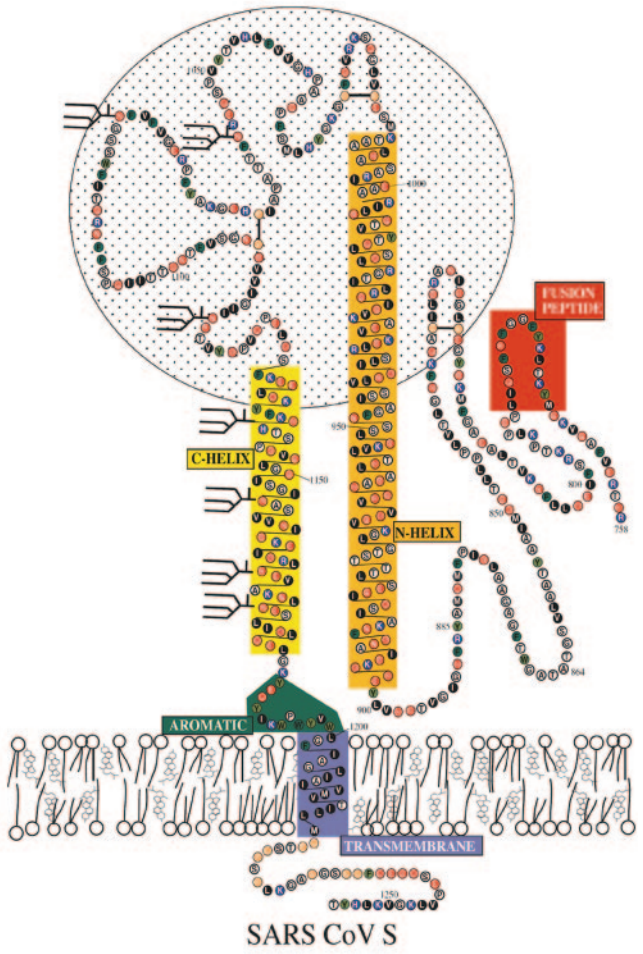

FIG. 7. Schematic of SARS-CoV S protein. The putative fusion peptide (red) is depicted at aa residues 770 to 788, 9 aa downstream of the minimum furin cleavage site (758R-N-T-R761). The two α-helical regions, N-helix (HR1, orange) and C-helix (HR2, yellow), are depicted at aa residues 902 to 1011 and 1131 to 1185, respectively. This is consistent with the HR predictions of Tripet et al. (84), Liu et al. (49), and Xu et al. (98). An interhelical domain of approximately 120 aa is depicted between the N- and C-helices. This region is extremely similar to the interhelical region of retrovirus TM proteins and EboV GP2 and has therefore been modeled as a similar disulfide-stabilized apex. Just prior to the transmembrane anchor (indigo) of S2, there is a region enriched in aromatic aa. This region, termed the aromatic domain (green), is highly conserved throughout the *Coronaviridae* and lies in an identical location to that of the aromatic domains of HIV and EboV. The S1 subunit, which includes the receptor-binding domain, is depicted schematically as a large ellipse, corresponding to the characteristic large globular head groups seen in electron micrographs of SARS-CoV.

the SARS-CoV S protein is proteolytically cleaved. It is important that while cleavage of the S protein of CoV appears to enhance fusion (35, 81), cleavage is not absolutely required for fusion (4, 5, 39, 75, 76).

Although the transition of the fusion protein core to the six-helix bundle conformation has been shown to mediate fusion by repositioning the cell and viral lipid membranes, the fusion peptide has been implicated as the mediator of the fusion process through its ability to induce the fusion and permeabilization of lipid membranes. We employed biophysical assays to identify which of the two possible SARS-CoV fusion peptides could partition into lipid membranes as well as induce fusion and permeabilization of lipid vesicles. These criteria were chosen based on the experimental approaches used to identify the fusion peptides of several other viral fusion proteins. Only $SARS_{WW-I}$ strongly partitioned into the lipid membranes of all LUV tested (Table 2). While $SARS_{WW-II}$ appeared to weakly bind to LUV composed of POPC and PI (9:1) (Fig. 2B), the calculated partition coefficient was significantly lower than that of $SARS_{WW-I}$ (Table 2). In a FRET fusion assay, we observed a rapid exponential increase in NBD fluorescence following the addition of $SARS_{WW-I}$, corresponding to 58% of the vesicles undergoing one fusion event at a P:L molar ratio of 1:10. In contrast, $SARS_{WW-II}$ caused a marginal increase in NBD fluorescence, indicative of fewer vesicles (~18%) undergoing membrane fusion events (Fig. 3 and Table 3). Even at a P:L ratio of 1:50, 38% of the vesicles underwent one fusion event in the presence of $SARS_{WW-I}$, whereas only 11% of vesicles underwent one fusion event in the presence of $SARS_{WW-II}$. The differences in fusion may correlate with the differing capacities of both peptides to partition into lipid membranes. While other studies have shown a correlation between a cation-mediated preaggregation of vesicles and peptide fusion activity (59, 64, 79), we observed no enhancement of NBD fluorescence for either $SARS_{WW-I}$ or $SARS_{WW-II}$ in the presence of 5 mM Ca^{2+}. Therefore, the peptide-mediated fusion observed was not dependent on a cation-mediated preaggregation of vesicles (data not shown).

When tested in the Tb^{3+}/DPA leakage assay, $SARS_{WW-I}$ induced measurable lipid vesicle permeabilization at all P:L ratios tested, whereas $SARS_{WW-II}$ induced minimal to no observable leakage (Fig. 5). Although both $SARS_{WW-I}$ and $SARS_{WW-II}$ showed similar propensities to interact with lipids based on their high interfacial hydrophobicities (Table 1), not all small hydrophobic peptides, even those with high WWIH scores, are capable of membrane disruption (94). Furthermore, the scrambled peptide of $SARS_{WW-I}$ did not interact with membranes (Fig. 2C and Table 2) and was unable to induce fusion (Fig. 4) or leakage (Fig. 5) of lipid vesicles, indicating that we measured a sequence-specific membrane disruption mediated by $SARS_{WW-I}$. The $SARS_{WW-I}$ peptide used throughout the aforementioned studies contained an aa substitution at residue 2 (Table 1), where the aromatic aa tyrosine was replaced with tryptophan. The rationale for this conservative aromatic aa replacement was that the intrinsic fluorescence of tryptophan is stronger and thus easier to quantitate spectrofluorometrically than that of tyrosine. To rule out the possibility that the capacity of $SARS_{WW-I}$ to induce both fusion and leakage of lipid vesicles was a consequence of the aromatic aa substitution, we tested an unmodified peptide in both the FRET fusion and Tb^{3+}/DPA leakage assays. As expected, the unmodified peptide exhibited activity identical to that of $SARS_{WW-I}$ in both assays (data not shown).

We also used CD spectroscopy to determine the propensity of the $SARS_{WW-I}$ peptide to adopt a defined secondary structure (α-helix or β-sheet) upon interaction with lipid membranes. Studies examining the secondary structures of viral fusion peptides have been conflicting. While numerous studies suggest that a predominantly α-helical structure is the single

fusion-active conformation adopted by viral fusion peptides (reviewed in reference 21), other studies argue that a β conformation is the active fusion state (1, 17, 65, 72, 80). CD analysis of the $SARS_{WW-I}$ peptide showed a propensity for the formation of a β-sheet structure in buffer and upon the addition of LUV (Fig. 6A). The formation of a β-sheet structure was independent of the presence of a cation, which has been shown to be necessary for the fusion peptides of EboV and HIV to assume a defined β-sheet secondary structure as well as to induce the aggregation and fusion of lipid vesicles (59, 80). The ability of the $SARS_{WW-I}$ peptide to adopt a secondary structure appears to be necessary for the peptide to interact with lipid membranes. Scrambling the peptide resulted in a loss of the β-sheet conformation (Fig. 6B) and an inability to bind to and interact with LUV. The secondary structure is a strongly driven thermodynamic consequence of membrane partitioning for hydrophobic peptides (90) which can be influenced by the peptide charge, aa organization, peptide-membrane surface density, lipid composition, and monolayer lateral pressure (79). Therefore, assumptions regarding the secondary structures of synthetic peptides are dependent on experimental conditions and are far from reflective of the true propensity of a viral fusion peptide to adopt a defined secondary structure in the context of the full glycoprotein. Nonetheless, CD analysis is a useful tool to study the behavior of these peptides in the context of model lipid membranes. The data presented herein for the SARS-CoV putative fusion peptide are consistent with the idea that the biologically relevant activity of viral fusion peptides is based on the propensity to adopt a defined secondary structure upon interaction with lipid membranes.

The biophysical studies presented above provide evidence that $SARS_{WW-I}$ behaves similarly to the synthetic viral fusion peptides of HIV, EboV, and influenza virus (14, 17, 21, 46, 58, 59, 62, 63, 65, 66, 70), in that the peptide has the capacity to partition into lipid membranes, adopt a well-defined secondary structure, and induce both fusion and permeabilization of lipid vesicles. The nominal P:L molar ratio was ~1:25 for both fusion and leakage assays; however, peptide binding assays demonstrated that at this molar ratio, ~40% of the peptide was actually bound to the lipid membrane under our experimental conditions. This suggests that less peptide is required to induce the observed levels of fusion and leakage. Observations that synthetic peptides corresponding to the fusion peptide domains of class I viral fusion proteins can induce measurable levels of fusion and leakage, separate from the context of the entire glycoprotein, provide support for models of viral fusion in which the fusion peptide and other domains actively facilitate lipid mixing (3, 73). The transition to the six-helix-bundle state may not only facilitate membrane juxtaposition but also function to align the fusion peptide with the aromatic domain and the transmembrane domain. The alignment of these three domains may then form a continuous track of hydrophobic, membrane-interacting surfaces that provide a low-energy (low-barrier) path for lipid flow and subsequent membrane fusion during the transition to or formation of the six-helix-bundle configuration (73).

Lastly, since the $SARS_{WW-II}$ peptide was capable of inducing one-third the amount of fusion and permeabilization of lipid vesicles that the $SARS_{WW-I}$ peptide induced, this less active sequence may work in conjunction with the $SARS_{WW-I}$ peptide or may constitute a second fusion peptide. Although its location within the S2 subunit is consistent with the position of the known internal fusion peptides of ASV and EboV, its inability to partition into lipid membranes (Fig. 2 and Table 2) and to adopt a well-defined secondary structure (data not shown) argues against the latter possibility. Although further mutagenesis studies need to be conducted to further verify the role of the $SARS_{WW-I}$ sequence in vitro, based on the biophysical assays presented above, we propose that residues 770 to 788 constitute the putative fusion peptide of the SARS-CoV S2 subunit. A working schematic of the SARS-CoV class I viral fusion protein, including the putative fusion peptide, the two well-characterized α-helices (HR1 and HR2), the transmembrane anchor, and other conserved structural domains present among many other class I viral fusion proteins, such as the aromatic domain and stem-loop region, is depicted in Fig. 7.

ACKNOWLEDGMENTS

This work was supported by the National Institutes of Health (AI054626, AI054238, RR018229, and CA08921 [R.F.G.] and GM60000 [W.C.W.]). Bruno Sainz is a recipient of a National Research Service Award from the National Institutes of Health (AIO543818).

ADDENDUM IN PROOF

In a very recent paper, Guillén et al. (J. Guillén, A. J. Pérez-Berná, M. R. Moreno, and J. Villalaín, J. Virol. **79:**1743–1752, 2005) describe experiments with overlapping peptides from the SARS-CoV S protein in which they show that peptides corresponding to the pre-TM aromatic domain and the region containing the WW-II segment cause moderate leakage from lipid vesicles at high peptide concentration. Based on this leakage data only, these authors suggest that the WW-II region may contain the S protein fusion peptide. We have observed similar levels of membrane disruption by these two sequences previously (73) and in this work and have also suggested a possible role for the aromatic domain and WW-II region in SARS-CoV S-protein-mediated membrane fusion. However, using direct measurements of binding, fusion, and membrane disruption, we have also shown here that the N-terminal WW-I region of the S2 protein has much more potent fusogenic and membrane disrupting activity than the other two sequences. We suggest that the WW-I sequence may be the primary fusion peptide, perhaps acting together with the WW-II region and the aromatic domain (73). Given the high interfacial hydrophobicity of the WW-I sequence, it is not clear why Guillén et al. observed no activity in their leakage experiments with corresponding peptides. However, none of the peptides they tested were identical in sequence to the WW-1 peptide used in the present study. The most similar peptides (105 and 106 in their series) were shifted 3 or 4 amino acids toward either the N or the C terminus, respectively (J. Villalaín, personal communication), suggesting that sequence details can determine membrane fusion activity of peptides. Our observation that a scrambled WW-I peptide has no activity supports this hypothesis.

REFERENCES

1. **Agirre, A., C. Flach, F. M. Goni, R. Mendelsohn, J. M. Valpuesta, F. Wu, and J. L. Nieva.** 2000. Interactions of the HIV-1 fusion peptide with large unilamellar vesicles and monolayers. A cryo-TEM and spectroscopic study. Biochim. Biophys. Acta **1467:**153–164.

2. **Bergeron, E., M. J. Vincent, L. Wickham, J. Hamelin, A. Basak, S. T. Nichol, M. Chretien, and N. G. Seidah.** 2005. Implication of proprotein convertases in the processing and spread of severe acute respiratory syndrome coronavirus. Biochem. Biophys. Res. Commun. **326:**554–563.
3. **Blumenthal, R., M. J. Clague, S. R. Durell, and R. M. Epand.** 2003. Membrane fusion. Chem. Rev. **103:**53–69.
4. **Bos, E. C., L. Heijnen, W. Luytjes, and W. J. Spaan.** 1995. Mutational analysis of the murine coronavirus spike protein: effect on cell-to-cell fusion. Virology **214:**453–463.
5. **Bos, E. C., W. Luytjes, and W. J. Spaan.** 1997. The function of the spike protein of mouse hepatitis virus strain A59 can be studied on virus-like particles: cleavage is not required for infectivity. J. Virol. **71:**9427–9433.
6. **Bosch, B. J., B. E. Martina, R. Van Der Zee, J. Lepault, B. J. Haijema, C. Versluis, A. J. Heck, R. De Groot, A. D. Osterhaus, and P. J. Rottier.** 2004. Severe acute respiratory syndrome coronavirus (SARS-CoV) infection inhibition using spike protein heptad repeat-derived peptides. Proc. Natl. Acad. Sci. USA **101:**8455–8460.
7. **Bosch, B. J., R. van der Zee, C. A. de Haan, and P. J. Rottier.** 2003. The coronavirus spike protein is a class I virus fusion protein: structural and functional characterization of the fusion core complex. J. Virol. **77:**8801–8811.
8. **Bosch, M. L., P. L. Earl, K. Fargnoli, S. Picciafuoco, F. Giombini, F. Wong-Staal, and G. Franchini.** 1989. Identification of the fusion peptide of primate immunodeficiency viruses. Science **244:**694–697.
9. **Bresnahan, P. A., R. Leduc, L. Thomas, J. Thorner, H. L. Gibson, A. J. Brake, P. J. Barr, and G. Thomas.** 1990. Human fur gene encodes a yeast KEX2-like endoprotease that cleaves pro-beta-NGF in vivo. J. Cell Biol. **111:**2851–2859.
10. **Caffrey, M., M. Cai, J. Kaufman, S. J. Stahl, P. T. Wingfield, D. G. Covell, A. M. Gronenborn, and G. M. Clore.** 1998. Three-dimensional solution structure of the 44 kDa ectodomain of SIV gp41. EMBO J. **17:**4572–4584.
11. **Carr, C. M., and P. S. Kim.** 1993. A spring-loaded mechanism for the conformational change of influenza hemagglutinin. Cell **73:**823–832.
12. **Cavanagh, D., and P. J. Davis.** 1986. Coronavirus IBV: removal of spike glycopolypeptide S1 by urea abolishes infectivity and haemagglutination but not attachment to cells. J. Gen. Virol. **67:**1443–1448.
13. **Chan, D. C., D. Fass, J. M. Berger, and P. S. Kim.** 1997. Core structure of gp41 from the HIV envelope glycoprotein. Cell **89:**263–273.
14. **Chang, D. K., S. F. Cheng, and W. J. Chien.** 1997. The amino-terminal fusion domain peptide of human immunodeficiency virus type 1 gp41 inserts into the sodium dodecyl sulfate micelle primarily as a helix with a conserved glycine at the micelle-water interface. J. Virol. **71:**6593–6602.
15. **Chang, D. K., S. F. Cheng, and V. D. Trivedi.** 1999. Biophysical characterization of the structure of the amino-terminal region of gp41 of HIV-1. Implications on viral fusion mechanism. J. Biol. Chem. **274:**5299–5309.
16. **Chen, P. S., T. Y. Toribara, and H. Warner.** 1956. Microdetermination of phosphorus. Anal. Chem. **28:**1756–1758.
17. **Davies, S. M., S. M. Kelly, N. C. Price, and J. P. Bradshaw.** 1998. Structural plasticity of the feline leukaemia virus fusion peptide: a circular dichroism study. FEBS Lett. **425:**415–418.
18. **de Haan, C. A., K. Stadler, G. J. Godeke, B. J. Bosch, and P. J. Rottier.** 2004. Cleavage inhibition of the murine coronavirus spike protein by a furin-like enzyme affects cell-cell but not virus-cell fusion. J. Virol. **78:**6048–6054.
19. **Delos, S. E., J. M. Gilbert, and J. M. White.** 2000. The central proline of an internal viral fusion peptide serves two important roles. J. Virol. **74:**1686–1693.
20. **Drosten, C., S. Gunther, W. Preiser, S. van der Werf, H. R. Brodt, S. Becker, H. Rabenau, M. Panning, L. Kolesnikova, R. A. Fouchier, A. Berger, A. M. Burguiere, J. Cinatl, M. Eickmann, N. Escriou, K. Grywna, S. Kramme, J. C. Manuguerra, S. Muller, V. Rickerts, M. Sturmer, S. Vieth, H. D. Klenk, A. D. Osterhaus, H. Schmitz, and H. W. Doerr.** 2003. Identification of a novel coronavirus in patients with severe acute respiratory syndrome. N. Engl. J. Med. **348:**1967–1976.
21. **Durell, S. R., I. Martin, J. M. Ruysschaert, Y. Shai, and R. Blumenthal.** 1997. What studies of fusion peptides tell us about viral envelope glycoprotein-mediated membrane fusion. Mol. Membr. Biol. **14:**97–112.
22. **Fiske, C. H., and Y. Subbarow.** 1925. The colorimetric determination of phosphorus. J. Biol. Chem. **66:**375–400.
23. **Freed, E. O., E. L. Delwart, G. L. Buchschacher, Jr., and A. T. Panganiban.** 1992. A mutation in the human immunodeficiency virus type 1 transmembrane glycoprotein gp41 dominantly interferes with fusion and infectivity. Proc. Natl. Acad. Sci. USA **89:**70–74.
24. **Freed, E. O., D. J. Myers, and R. Risser.** 1990. Characterization of the fusion domain of the human immunodeficiency virus type 1 envelope glycoprotein gp41. Proc. Natl. Acad. Sci. USA **87:**4650–4654.
25. **Gallagher, T. M., and M. J. Buchmeier.** 2001. Coronavirus spike proteins in viral entry and pathogenesis. Virology **279:**371–374.
26. **Gallaher, W. R.** 1987. Detection of a fusion peptide sequence in the transmembrane protein of human immunodeficiency virus. Cell **50:**327–328.
27. **Gallaher, W. R.** 1996. Similar structural models of the transmembrane proteins of Ebola and avian sarcoma viruses. Cell **85:**477–478.
28. **Gallaher, W. R., J. M. Ball, R. F. Garry, M. C. Griffin, and R. C. Montelaro.** 1989. A general model for the transmembrane proteins of HIV and other retroviruses. AIDS Res. Hum. Retrovir. **5:**431–440.
29. **Gallaher, W. R., and R. F. Garry.** 2003. Model of the pre-insertion region of the spike (S2) fusion glycoprotein of the human SARS coronavirus: implications for antiviral therapeutics. [Online.] http://www.virology.net/Articles/sars/s2model.html.
30. **Gallaher, W. R., J. P. Segrest, and E. Hunter.** 1992. Are fusion peptides really "sided" insertional helices? Cell **70:**531–532.
31. **Garry, R. F., and S. Dash.** 2003. Proteomics computational analyses suggest that hepatitis C virus E1 and pestivirus E2 envelope glycoproteins are truncated class II fusion proteins. Virology **307:**255–265.
32. **Gething, M. J., R. W. Doms, D. York, and J. White.** 1986. Studies on the mechanism of membrane fusion: site-specific mutagenesis of the hemagglutinin of influenza virus. J. Cell Biol. **102:**11–23.
33. **Goldsmith, C. S., K. M. Tatti, T. G. Ksiazek, P. E. Rollin, J. A. Comer, W. W. Lee, P. A. Rota, B. Bankamp, W. J. Bellini, and S. R. Zaki.** 2004. Ultrastructural characterization of SARS coronavirus. Emerg. Infect. Dis. **10:**320–326.
34. **Gomara, M. J., P. Mora, I. Mingarro, and J. L. Nieva.** 2004. Roles of a conserved proline in the internal fusion peptide of Ebola glycoprotein. FEBS Lett. **569:**261–266.
35. **Gombold, J. L., S. T. Hingley, and S. R. Weiss.** 1993. Fusion-defective mutants of mouse hepatitis virus A59 contain a mutation in the spike protein cleavage signal. J. Virol. **67:**4504–4512.

35a. **Guillén J., A. J. Pérez-Berná, M. R. Moreno, and J. Villalaín.** 2005. Identification of the membrane-active regions of the severe acute respiratory syndrome coronavirus spike membrane glycoprotein using a 16/18-mer peptide scan: implications for the viral fusion mechanism. J. Virol. **79:**1743–1752.

36. **Harter, C., P. James, T. Bachi, G. Semenza, and J. Brunner.** 1989. Hydrophobic binding of the ectodomain of influenza hemagglutinin to membranes occurs through the "fusion peptide". J. Biol. Chem. **264:**6459–6464.
37. **Hernandez, L. D., L. R. Hoffman, T. G. Wolfsberg, and J. M. White.** 1996. Virus-cell and cell-cell fusion. Annu. Rev. Cell Dev. Biol. **12:**627–661.
38. **Hernandez, L. D., and J. M. White.** 1998. Mutational analysis of the candidate internal fusion peptide of the avian leukosis and sarcoma virus subgroup A envelope glycoprotein. J. Virol. **72:**3259–3267.
39. **Hingley, S. T., I. Leparc-Goffart, and S. R. Weiss.** 1998. The spike protein of murine coronavirus mouse hepatitis virus strain A59 is not cleaved in primary glial cells and primary hepatocytes. J. Virol. **72:**1606–1609.
40. **Hoffman, K., and W. Stoffel.** 1993. TMbase—a database of membrane-spanning segments. Biol. Chem. Hoppe-Seyler **374:**166–170.
41. **Horvath, C. M., and R. A. Lamb.** 1992. Studies on the fusion peptide of a paramyxovirus fusion glycoprotein: roles of conserved residues in cell fusion. J. Virol. **66:**2443–2455.
42. **Hunter, E., E. Hill, M. Hardwick, A. Bhown, D. E. Schwartz, and R. Tizard.** 1983. Complete sequence of the Rous sarcoma virus *env* gene: identification of structural and functional regions of its product. J. Virol. **46:**920–936.
43. **Ito, H., S. Watanabe, A. Sanchez, M. A. Whitt, and Y. Kawaoka.** 1999. Mutational analysis of the putative fusion domain of Ebola virus glycoprotein. J. Virol. **73:**8907–8912.
44. **Jeffers, S. A., S. M. Tusell, L. Gillim-Ross, E. M. Hemmila, J. E. Achenbach, G. J. Babcock, W. D. Thomas, Jr., L. B. Thackray, M. D. Young, R. J. Mason, D. M. Ambrosino, D. E. Wentworth, J. C. Demartini, and K. V. Holmes.** 2004. CD209L (L-SIGN) is a receptor for severe acute respiratory syndrome coronavirus. Proc. Natl. Acad. Sci. USA **101:**15748–15753.
45. **Ksiazek, T. G., D. Erdman, C. S. Goldsmith, S. R. Zaki, T. Peret, S. Emery, S. Tong, C. Urbani, J. A. Comer, W. Lim, P. E. Rollin, S. F. Dowell, A. E. Ling, C. D. Humphrey, W. J. Shieh, J. Guarner, C. D. Paddock, P. Rota, B. Fields, J. DeRisi, J. Y. Yang, N. Cox, J. M. Hughes, J. W. LeDuc, W. J. Bellini, and L. J. Anderson.** 2003. A novel coronavirus associated with severe acute respiratory syndrome. N. Engl. J. Med. **348:**1953–1966.
46. **Lear, J. D., and W. F. DeGrado.** 1987. Membrane binding and conformational properties of peptides representing the NH2 terminus of influenza HA-2. J. Biol. Chem. **262:**6500–6505.
47. **Lee, H. J., C. K. Shieh, A. E. Gorbalenya, E. V. Koonin, N. La Monica, J. Tuler, A. Bagdzhadzhyan, and M. M. Lai.** 1991. The complete sequence (22 kilobases) of murine coronavirus gene 1 encoding the putative proteases and RNA polymerase. Virology **180:**567–582.
48. **Li, W., M. J. Moore, N. Vasilieva, J. Sui, S. K. Wong, M. A. Berne, M. Somasundaran, J. L. Sullivan, K. Luzuriaga, T. C. Greenough, H. Choe, and M. Farzan.** 2003. Angiotensin-converting enzyme 2 is a functional receptor for the SARS coronavirus. Nature **426:**450–454.
49. **Liu, S., G. Xiao, Y. Chen, Y. He, J. Niu, C. R. Escalante, H. Xiong, J. Farmar, A. K. Debnath, P. Tien, S. Jiang, C. S. Goldsmith, K. M. Tatti, T. G. Ksiazek, P. E. Rollin, J. A. Comer, W. W. Lee, P. A. Rota, B. Bankamp, W. J. Bellini, and S. R. Zaki.** 2004. Interaction between heptad repeat 1 and 2 regions in spike protein of SARS-associated coronavirus: implications for virus fusogenic mechanism and identification of fusion inhibitors. Lancet **363:**938–947.
50. **Luo, Z., and S. R. Weiss.** 1998. Roles in cell-to-cell fusion of two conserved hydrophobic regions in the murine coronavirus spike protein. Virology **244:**483–494.
51. **Luo, Z. L., and S. R. Weiss.** 1998. Mutational analysis of fusion peptide-like

regions in the mouse hepatitis virus strain A59 spike protein. Adv. Exp. Med. Biol. **440:**17–23.
52. **Luytjes, W., L. S. Sturman, P. J. Bredenbeek, J. Charite, B. A. van der Zeijst, M. C. Horzinek, and W. J. Spaan.** 1987. Primary structure of the glycoprotein E2 of coronavirus MHV-A59 and identification of the trypsin cleavage site. Virology **161:**479–487.
53. **Malashkevich, V. N., D. C. Chan, C. T. Chutkowski, and P. S. Kim.** 1998. Crystal structure of the simian immunodeficiency virus (SIV) gp41 core: conserved helical interactions underlie the broad inhibitory activity of gp41 peptides. Proc. Natl. Acad. Sci. USA **95:**9134–9139.
54. **Mayer, L. D., M. J. Hope, and P. R. Cullis.** 1986. Vesicles of variable sizes produced by a rapid extrusion procedure. Biochim. Biophys. Acta **858:**161–168.
55. **Molloy, S. S., P. A. Bresnahan, S. H. Leppla, K. R. Klimpel, and G. Thomas.** 1992. Human furin is a calcium-dependent serine endoprotease that recognizes the sequence Arg-X-X-Arg and efficiently cleaves anthrax toxin protective antigen. J. Biol. Chem. **267:**16396–16402.
56. **Nayar, R., M. J. Hope, and P. R. Cullis.** 1989. Generation of large unilamellar vesicles from long-chain saturated phosphatidylcholines by extrusion technique. Biochim. Biophys. Acta **986:**200–206.
57. **Nichols, J. W., and R. E. Pagano.** 1982. Use of resonance energy transfer to study the kinetics of amphiphile transfer between vesicles. Biochemistry **21:**1720–1726.
58. **Nieva, J. L., and A. Agirre.** 2003. Are fusion peptides a good model to study viral cell fusion? Biochim. Biophys. Acta **1614:**104–115.
59. **Nieva, J. L., S. Nir, A. Muga, F. M. Goni, and J. Wilschut.** 1994. Interaction of the HIV-1 fusion peptide with phospholipid vesicles: different structural requirements for fusion and leakage. Biochemistry **33:**3201–3209.
60. **Peiris, J. S., S. T. Lai, L. L. Poon, Y. Guan, L. Y. Yam, W. Lim, J. Nicholls, W. K. Yee, W. W. Yan, M. T. Cheung, V. C. Cheng, K. H. Chan, D. N. Tsang, R. W. Yung, T. K. Ng, and K. Y. Yuen.** 2003. Coronavirus as a possible cause of severe acute respiratory syndrome. Lancet **361:**1319–1325.
61. **Peisajovich, S. G., and Y. Shai.** 2003. Viral fusion proteins: multiple regions contribute to membrane fusion. Biochim. Biophys. Acta **1614:**122–129.
62. **Pereira, F. B., F. M. Goni, A. Muga, and J. L. Nieva.** 1997. Permeabilization and fusion of uncharged lipid vesicles induced by the HIV-1 fusion peptide adopting an extended conformation: dose and sequence effects. Biophys. J. **73:**1977–1986.
63. **Pereira, F. B., J. M. Valpuesta, G. Basanez, F. M. Goni, and J. L. Nieva.** 1999. Interbilayer lipid mixing induced by the human immunodeficiency virus type-1 fusion peptide on large unilamellar vesicles: the nature of the nonlamellar intermediates. Chem. Phys. Lipids **103:**11–20.
64. **Pritsker, M., J. Rucker, T. L. Hoffman, R. W. Doms, and Y. Shai.** 1999. Effect of nonpolar substitutions of the conserved Phe11 in the fusion peptide of HIV-1 gp41 on its function, structure, and organization in membranes. Biochemistry **38:**11359–11371.
65. **Rafalski, M., J. D. Lear, and W. F. DeGrado.** 1990. Phospholipid interactions of synthetic peptides representing the N-terminus of HIV gp41. Biochemistry **29:**7917–7922.
66. **Rafalski, M., A. Ortiz, A. Rockwell, L. C. van Ginkel, J. D. Lear, W. F. DeGrado, and J. Wilschut.** 1991. Membrane fusion activity of the influenza virus hemagglutinin: interaction of HA2 N-terminal peptides with phospholipid vesicles. Biochemistry **30:**10211–10220.
67. **Rausch, J. M., and W. C. Wimley.** 2001. A high-throughput screen for identifying transmembrane pore-forming peptides. Anal. Biochem. **293:**258–263.
68. **Rockwell, N. C., D. J. Krysan, T. Komiyama, and R. S. Fuller.** 2002. Precursor processing by kex2/furin proteases. Chem. Rev. **102:**4525–4548.
69. **Rota, P. A., M. S. Oberste, S. S. Monroe, W. A. Nix, R. Campagnoli, J. P. Icenogle, S. Penaranda, B. Bankamp, K. Maher, M. H. Chen, S. Tong, A. Tamin, L. Lowe, M. Frace, J. L. DeRisi, Q. Chen, D. Wang, D. D. Erdman, T. C. Peret, C. Burns, T. G. Ksiazek, P. E. Rollin, A. Sanchez, S. Liffick, B. Holloway, J. Limor, K. McCaustland, M. Olsen-Rasmussen, R. Fouchier, S. Gunther, A. D. Osterhaus, C. Drosten, M. A. Pallansch, L. J. Anderson, and W. J. Bellini.** 2003. Characterization of a novel coronavirus associated with severe acute respiratory syndrome. Science **300:**1394–1399.
70. **Ruiz-Arguello, M. B., F. M. Goni, F. B. Pereira, and J. L. Nieva.** 1998. Phosphatidylinositol-dependent membrane fusion induced by a putative fusogenic sequence of Ebola virus. J. Virol. **72:**1775–1781.
71. **Saez-Cirion, A., M. J. Gomara, A. Agirre, and J. L. Nieva.** 2003. Pre-transmembrane sequence of Ebola glycoprotein. Interfacial hydrophobicity distribution and interaction with membranes. FEBS Lett. **533:**47–53.
72. **Saez-Cirion, A., and J. L. Nieva.** 2002. Conformational transitions of membrane-bound HIV-1 fusion peptide. Biochim. Biophys. Acta **1564:**57–65.
73. **Sainz, B., Jr., J. M. Rausch, W. R. Gallaher, R. F. Garry, and W. C. Wimley.** 2005. The aromatic domain of the coronavirus class I viral fusion protein induces membrane permeabilization: putative role during viral entry. Biochemistry **44:**947–958.
74. **Spaan, W., D. Cavanagh, and M. C. Horzinek.** 1988. Coronaviruses: structure and genome expression. J. Gen. Virol. **69:**2939–2952.
75. **Stauber, R., M. Pfleiderer, and S. Siddell.** 1993. Proteolytic cleavage of the murine coronavirus surface glycoprotein is not required for its fusion activity. Adv. Exp. Med. Biol. **342:**165–170.
76. **Stauber, R., M. Pfleiderera, and S. Siddell.** 1993. Proteolytic cleavage of the murine coronavirus surface glycoprotein is not required for fusion activity. J. Gen. Virol. **74:**183–191.
77. **Struck, D. K., D. Hoekstra, and R. E. Pagano.** 1981. Use of resonance energy transfer to monitor membrane fusion. Biochemistry **20:**4093–4099.
78. **Suarez, T., W. R. Gallaher, A. Agirre, F. M. Goni, and J. L. Nieva.** 2000. Membrane interface-interacting sequences within the ectodomain of the human immunodeficiency virus type 1 envelope glycoprotein: putative role during viral fusion. J. Virol. **74:**8038–8047.
79. **Suarez, T., M. J. Gomara, F. M. Goni, I. Mingarro, A. Muga, E. Perez-Paya, and J. L. Nieva.** 2003. Calcium-dependent conformational changes of membrane-bound Ebola fusion peptide drive vesicle fusion. FEBS Lett. **535:**23–28.
80. **Suarez, T., S. Nir, F. M. Goni, A. Saez-Cirion, and J. L. Nieva.** 2000. The pre-transmembrane region of the human immunodeficiency virus type-1 glycoprotein: a novel fusogenic sequence. FEBS Lett. **477:**145–149.
81. **Taguchi, F.** 1993. Fusion formation by the uncleaved spike protein of murine coronavirus JHMV variant cl-2. J. Virol. **67:**1195–1202.
82. **Taguchi, F.** 1995. The S2 subunit of the murine coronavirus spike protein is not involved in receptor binding. J. Virol. **69:**7260–7263.
83. **Taguchi, F., and Y. K. Shimazaki.** 2000. Functional analysis of an epitope in the S2 subunit of the murine coronavirus spike protein: involvement in fusion activity. J. Gen. Virol. **81:**2867–2871.
84. **Tripet, B., M. W. Howard, M. Jobling, R. K. Holmes, K. V. Holmes, and R. S. Hodges.** 2004. Structural characterization of the SARS-coronavirus spike S fusion protein core. J. Biol. Chem. **279:**20836–20849.
85. **Wang, P., J. Chen, A. Zheng, Y. Nie, X. Shi, W. Wang, G. Wang, M. Luo, H. Liu, L. Tan, X. Song, Z. Wang, X. Yin, X. Qu, X. Wang, T. Qing, M. Ding, and H. Deng.** 2004. Expression cloning of functional receptor used by SARS coronavirus. Biochem. Biophys. Res. Commun. **315:**439–444.
86. **Weissenhorn, W., A. Carfi, K. H. Lee, J. J. Skehel, and D. C. Wiley.** 1998. Crystal structure of the Ebola virus membrane fusion subunit, GP2, from the envelope glycoprotein ectodomain. Mol. Cell **2:**605–616.
87. **Weissenhorn, W., A. Dessen, S. C. Harrison, J. J. Skehel, and D. C. Wiley.** 1997. Atomic structure of the ectodomain from HIV-1 gp41. Nature **387:**426–430.
88. **White, J., M. Kielian, and A. Helenius.** 1983. Membrane fusion proteins of enveloped animal viruses. Q. Rev. Biophys. **16:**151–195.
89. **White, J. M.** 1992. Membrane fusion. Science **258:**917–924.
90. **White, S. H., and W. C. Wimley.** 1999. Membrane protein folding and stability: physical principles. Annu. Rev. Biophys. Biomol. Struct. **28:**319–365.
91. **White, S. H., W. C. Wimley, A. S. Ladokhin, and K. Hristova.** 1998. Protein folding in membranes: determining energetics of peptide-bilayer interactions. Methods Enzymol. **295:**62–87.
92. **Wilson, I. A., J. J. Skehel, and D. C. Wiley.** 1981. Structure of the haemagglutinin membrane glycoprotein of influenza virus at 3 A resolution. Nature **289:**366–373.
93. **Wimley, W. C., K. Hristova, A. S. Ladokhin, L. Silvestro, P. H. Axelsen, and S. H. White.** 1998. Folding of beta-sheet membrane proteins: a hydrophobic hexapeptide model. J. Mol. Biol. **277:**1091–1110.
94. **Wimley, W. C., and S. H. White.** 1996. Experimentally determined hydrophobicity scale for proteins at membrane interfaces. Nat. Struct. Biol. **3:**842–848.
95. **Wong, S. K., W. Li, M. J. Moore, H. Choe, and M. Farzan.** 2004. A 193-amino acid fragment of the SARS coronavirus S protein efficiently binds angiotensin-converting enzyme 2. J. Biol. Chem. **279:**3197–3201.
96. **Wu, X. D., B. Shang, R. F. Yang, H. Yu, Z. H. Ma, X. Shen, Y. Y. Ji, Y. Lin, Y. D. Wu, G. M. Lin, L. Tian, X. Q. Gan, S. Yang, W. H. Jiang, E. H. Dai, X. Y. Wang, H. L. Jiang, Y. H. Xie, X. L. Zhu, G. Pei, L. Li, J. R. Wu, and B. Sun.** 2004. The spike protein of severe acute respiratory syndrome (SARS) is cleaved in virus infected Vero-E6 cells. Cell Res. **14:**400–406.
97. **Xu, Y., Y. Liu, Z. Lou, L. Qin, X. Li, Z. Bai, H. Pang, P. Tien, G. F. Gao, and Z. Rao.** 2004. Structural basis for coronavirus-mediated membrane fusion. Crystal structure of mouse hepatitis virus spike protein fusion core. J. Biol. Chem. **279:**30514–30522.
98. **Xu, Y., Z. Lou, Y. Liu, H. Pang, P. Tien, G. F. Gao, and Z. Rao.** 2004. Crystal structure of severe acute respiratory syndrome coronavirus spike protein fusion core. J. Biol. Chem. **279:**49414–49419.
99. **Zhu, J., G. Xiao, Y. Xu, F. Yuan, C. Zheng, Y. Liu, H. Yan, D. K. Cole, J. I. Bell, Z. Rao, P. Tien, and G. F. Gao.** 2004. Following the rule: formation of the 6-helix bundle of the fusion core from severe acute respiratory syndrome coronavirus spike protein and identification of potent peptide inhibitors. Biochem. Biophys. Res. Commun. **319:**283–288.